

A discrete vortex method for the non-steady separated flow over an airfoil

By J. KATZ†

Ames Research Center, NASA, Moffett Field, California 94035

(Received 20 December 1979 and in revised form 4 March 1980)

A discrete vortex method was used to analyse the separated non-steady flow about a cambered airfoil. The foil flow modelling is based on the thin lifting-surface approach, where the chordwise location of the separation point is assumed to be known from experiments or flow-visualization data. Calculated results provided good agreement when compared with the post-stall aerodynamic data of two airfoils. Those airfoil sections differed in the extent of travel of the separation point with increasing angle of attack. Furthermore, the periodic wake shedding was analysed and its time-dependent influence on the airfoil was investigated.

1. Introduction

The post-stall aerodynamic behaviour of straight-wing General Aviation aircraft has recently been a subject of increased interest. This has been partially due to the increased number of stall and spin accidents where the partially stalled lifting surfaces might cause the loss of lateral control. In order to reduce spin-entry tendencies, several methods have been applied. One of these methods was investigated by Feistel, Anderson & Kroeger (1978), who tried to reduce post-stall rolling moments by prescribing local wing separation in a predetermined manner. It was found in these studies that standard analytical techniques to predict the influence of partially separated section on the attached regions of a straight leading-edge wing were inadequate. Therefore, the present work is concentrated on developing a two-dimensional vortex lattice method (VLM) to simulate two-dimensional airfoil data. This can provide the strength and wake geometrical structure to a three-dimensional VLM to allow the calculation of the influence of the wing-separated section on the non-separated regions.

Discrete-vortex methods have been used by numerous authors, and a list of the application of these methods is included in Clements & Maull (1975) and Sarpkaya (1979). The separated non-steady wake shedding behind cylindrical bodies is still being widely investigated. Marshall & Deffenbaugh (1974) calculated the three-dimensional separated flow behind cylinders by solving the crossflow problem via the discrete vortex method. Mendenhall, Spangler & Perkins (1979) used a similar technique to determine the crossflow around circular and non-circular bodies. They applied the Stratford (1959) criteria for the prediction of the separation point. The wake dynamics of separated flow behind a cylinder were studied by Sarpkaya & Shoaff (1979). They introduced a rediscrretization method for wake roll-up and a circulation reduction scheme to bring calculated results closer to experimental observations.

† NRC Associate. Present address: Dept. Mechanical Engineering, Technion, Haifa, Israel.

The principles of the discrete vortex method for modelling airfoils with boundary-layer separation were summarized by Sears (1976). The vortex shedding behind a flat plate was analysed by Sarpkaya (1975), who calculated the strength of the emanating vorticity layers by the shear velocity method, observed experimentally by Fage & Johansen (1927). A different method for the calculation of the strength of shed vorticity was applied by Kiya & Arie (1977). They introduced the nascent vortices at a fixed location, while its strength was calculated by the Kutta condition. The literature cited above shows the effort conducted to reduce the viscous problem into a simpler potential model. However, there are codes like the one developed by Mehta (1977) which are based on the solution of the Navier–Stokes equations. The major drawbacks of these codes are the large computer times and memory required relative to the time and memory for the much simpler discrete-vortex methods. The present work is an extension of the discrete-vortex methods that account for camber effects and for cases where the frontal separation point is significantly behind the leading edge. This type of separation is more realistic for the modelling of the post-stall aerodynamics of airfoils with rounded leading edges and can lead to better agreements with experimental results.

2. Analytical model

One of the major reasons for the success of the potential theory approach for the solution of the flow field around an attached airfoil is the introduction of the Kutta condition. This condition determines the circulation generated at the viscous shear layer on the foil by requiring zero circulation at a given location (the trailing edge, in the case of airfoils). That approach can be extended further to allow the study of the flow around separated airfoils. In this case, an additional shear layer emanates from a given point on the airfoil surface. The strength and the location of this second separation point is then to be supplied. This approach was successfully applied by several authors, such as Sarpkaya (1975) or Kiya & Arie (1977) who placed the separation point of a flat plate at its leading edge.

In the present study, the separation point location is not necessarily at the leading edge. It is assumed that the location of the separation point, which is a function of foil curvature and Reynolds number (laminar or turbulent), is known from experiments, flow visualization (McAlister & Carr 1978) or independent calculation schemes. Such schemes were used by Mendenhall *et al.* (1979) and Sarpkaya & Shoaff (1979) for the study of separated flow behind cylinders. They used separation criteria based on the local pressure gradient such as the Stratford (1959) criteria. Since the location of the separation point is assumed to be known, only the thin wing lifting problem is analysed. A further extension of the present work might include airfoil thickness to allow the additional calculation of the separation point location for the given Reynolds number and foil geometry.

The above considerations lead to the definition of the thin cambered wing problem (figure 1) with a known separation point X_{sep} (which is the time-average position of the oscillatory motion). Furthermore, it is assumed that the surrounding fluid is incompressible, and irrotational over the whole region, excluding the wing and its wake elements.

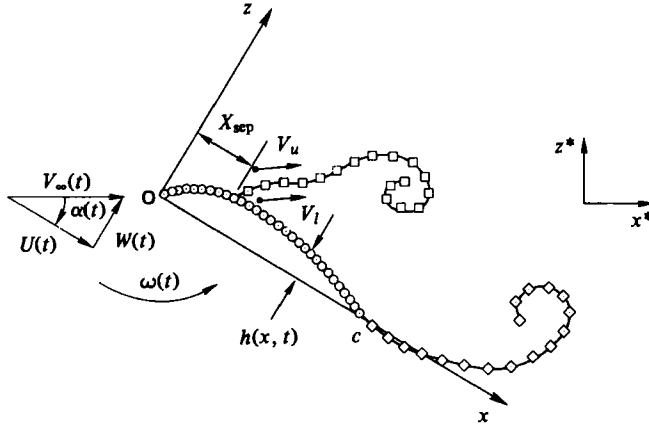


FIGURE 1. Schematic description of model.

The continuity equation in that region is defined in a stationary co-ordinate system (x^*-z^* (figure 1)):

$$\nabla^2 \phi^* = 0 \tag{1}$$

where ϕ^* is the time-dependent velocity potential, consisting of the foil potential ϕ_0^* , wake potential ϕ_w^* , and the separated shear-layer potential ϕ_s^* .

$$\phi(x^*, z^*, t^*) = \phi_0^* + \phi_w^* + \phi_s^* \equiv \phi^*. \tag{2}$$

The boundary conditions for equation (1) are as follows.

(a) There is no flow through the foil surface $z^* = h(x^*, t^*) \equiv h^*$,

$$\left. \frac{\partial \phi^*}{\partial z^*} \right|_{\text{on foil}} = \frac{\partial \phi^*}{\partial x^*} \frac{\partial h^*}{\partial x^*} + \frac{\partial h^*}{\partial t^*}, \tag{3}$$

where h^* stands for the momentary camber of the wing, as indicated in figure 1.

(b) The velocity induced by the foil motion decays far from the foil:

$$\nabla \phi^* = 0 \quad \text{as} \quad |x^*|, |z^*| \rightarrow \infty. \tag{4}$$

In addition, the momentary strength of the two emanating shear layers is to be calculated. The circulation shed at the separation point X_{sep} can be calculated by performing the line integral of equation (5) enclosing a portion of the wake behind X_{sep} , but not crossing the foil,

$$\frac{d\Gamma_s}{dt} = \frac{D}{Dt} \oint \mathbf{V} \cdot d\mathbf{s} \tag{5}$$

where Γ_s is the separated wake circulation, \mathbf{V} is the velocity vector, and $d\mathbf{s}$ is a path element along the integration curve. This integral might be calculated at any momentarily non-rotating co-ordinate system, such as the foil-attached $x-z$ system. By assuming the existence of average velocities V_u and V_l (figure 1) at the upper and lower edges of the shear layer, an approximate expression can be derived:

$$\frac{d\Gamma_s}{dt} = \frac{d}{dt} (V_u ds - V_l ds) \simeq \frac{1}{2} (V_u^2 - V_l^2). \tag{6}$$

The validity of this simple expression was demonstrated experimentally by Fage & Johansen (1927), and it was used successfully in discrete vortex methods by

numerous authors, e.g. Mendenhall *et al.* (1979), Marshall & Deffenbaugh (1974) and Sarpkaya (1975, 1979).

The instantaneous strength of the vortex sheet, shed at the trailing edge, is to be calculated by Kelvin's theorem:

$$\frac{d\Gamma}{dt} = \frac{d\Gamma_f}{dt} + \frac{d\Gamma_w}{dt} + \frac{d\Gamma_s}{dt} = 0 \quad (\text{for all } t), \quad (7)$$

where Γ_f and Γ_w are the foil and wake circulations, respectively. The above order of obtaining the strength of the two shear layers by equations (5) and (7) was chosen as a result of computer programming convenience. However, a reversed order for this solution might be used, thus $d\Gamma_w/dt$ would be calculated by applying equation (5) at the trailing edge and then $d\Gamma_s/dt$ is determined from equation (7).

The momentary pressure is calculated by the time-dependent Bernoulli's equation:

$$\frac{p_\infty - p}{\rho} = -\frac{1}{2} \left[\left(\frac{\partial \phi^*}{\partial x^*} \right)^2 + \left(\frac{\partial \phi^*}{\partial z^*} \right)^2 \right] + \frac{\partial \phi^*}{\partial t^*}. \quad (8)$$

In order to attain a simplified solution of the boundary-value problem of equations (1)–(4), it is to be stated in the x - z co-ordinate system which might rotate at the angular velocity ω . That is done following the transformation suggested by Katz & Weihs (1978) resulting in the following relations between the derivatives of the two co-ordinate systems:

$$\left. \begin{aligned} \frac{\partial}{\partial x^*} &= \cos \alpha \frac{\partial}{\partial x} + \sin \alpha \frac{\partial}{\partial z}, \\ \frac{\partial}{\partial z^*} &= -\sin \alpha \frac{\partial}{\partial x} + \cos \alpha \frac{\partial}{\partial z}, \\ \frac{\partial}{\partial t^*} &= [z\omega + U(t)] \frac{\partial}{\partial x} - [x\omega - W(t)] \frac{\partial}{\partial z} + \frac{\partial}{\partial t}, \end{aligned} \right\} \quad (9)$$

where α is the foil momentary angle of attack, and $U(t)$, $W(t)$ are the components of the far velocity $V_\infty(t)$ to the direction of the x , z co-ordinates, respectively.

The transformed continuity equation is:

$$\nabla^2 \phi = 0, \quad (10)$$

$$\phi(x, z, t) = \phi_0 + \phi_w + \phi_s \equiv \phi. \quad (11)$$

However, the velocity potentials ϕ_w and ϕ_s consist of discrete vortices whose strengths are calculated at previous time steps, while the latest two nascent vortices are calculated by equations (6) and (7). Therefore, the only unknown part of the potential ϕ is ϕ_0 that has to fulfill the continuity equation:

$$\nabla^2 \phi_0 = 0. \quad (12)$$

The transformed boundary conditions are

$$\left. \frac{\partial \phi_0}{\partial z} \right|_{z=0} = \left[U(t) + \frac{\partial \phi_0}{\partial x} + \frac{\partial \phi_w}{\partial x} + \frac{\partial \phi_s}{\partial x} \right] \frac{\partial h}{\partial x} + \frac{\partial h}{\partial t} + [x\omega - W(t)] - \left[\frac{\partial \phi_w}{\partial z} + \frac{\partial \phi_s}{\partial z} \right]. \quad (13)$$

Here it was assumed that the momentary local camberline $h(x, t)$ is much smaller than the foil chord c ($h/c \ll 1$). Therefore, boundary condition (13) is fulfilled along the x co-ordinate ($z = 0$). The transformed equation (4) becomes:

$$\nabla\phi_0 = 0 \quad \text{as} \quad |x|, |z| \rightarrow \infty. \quad (14)$$

That condition actually doesn't change because the velocity potential ϕ is defined in the x^*-z^* system and the transformation is used only to define the boundary condition in a more convenient system.

The transformed Bernoulli equation is

$$\frac{p_\infty - p}{\rho} = \left\{ [z\omega + U(t)] \frac{\partial}{\partial x} - [x\omega - W(t)] \frac{\partial}{\partial z} + \frac{\partial}{\partial t} \right\} \phi - \frac{1}{2} \left[\left(\frac{\partial\phi}{\partial x} \right)^2 + \left(\frac{\partial\phi}{\partial z} \right)^2 \right]. \quad (15)$$

The solution of equations (10) through (14) can be obtained by representing the foil with distributed vortices along the chord line. The strength of this vortex sheet can be solved by assuming discrete vortices (vortex lattice) or by a continuous vortex distribution, stated in terms of the following Fourier equation:

$$\gamma(\theta, t) = 2V_\infty(t) \left[A_0(t) \frac{1 + \cos\theta}{\sin\theta} + \sum_{n=1}^{\infty} A_n(t) \sin(n\theta) \right], \quad (16)$$

$$x = \frac{c}{2} (1 - \cos\theta). \quad (17)$$

The above vortex distribution includes the suction peak-term coefficient A_0 . This is included because most airfoils have rounded leading edges and sharp trailing edges, therefore some portion of the suction peak (ahead of the separation point) exists even at very high angles of attack. This phenomenon was shown experimentally in several works, such as Pinkerton (1937) or McCullough & Gault (1951). However, in the case of symmetrical trailing and leading edges, and while the foil is perpendicular to the flow, the coefficient A_0 should be neglected.

The Kutta condition at the trailing edge (18) is already fulfilled in equation (16):

$$\gamma(c, t) = 0. \quad (18)$$

There are no further requirements for the complete solution of the problem, however, additional 'Kutta-type' conditions might be added at the frontal separation point to boost wake-shedding oscillations.

By substituting equations (16) and (17) into boundary condition (13), the solution of the Fourier coefficients is obtained:

$$A_0(t) = \frac{-1}{\pi} \int_0^\pi \frac{1}{V_\infty} \left(\frac{\partial\phi_0}{\partial z} \right)_{z=0} d\theta, \quad (19)$$

$$A_n(t) = \frac{2}{\pi} \int_0^\pi \frac{1}{V_\infty} \left(\frac{\partial\phi_0}{\partial z} \right)_{z=0} \cos(n\theta) d\theta \quad (n \geq 1). \quad (20)$$

These integrals can be performed for a given chordwise downwash distribution $(\partial\phi/\partial z)_{z=0}$ of equation (13).

The normal force distribution dF/dx is obtained from equation (15) by omitting the symmetrical pressure terms that do not contribute to the lift,

$$\frac{dF}{dx} = p^- - p^+ = 2\rho \left[\frac{\partial\phi}{\partial t} + U(t) \frac{\partial\phi}{\partial x} \right] + \frac{\rho}{2} \Delta, \quad (21)$$

$$\Delta = \left[\left(\frac{\partial\phi}{\partial x} \right)^2 + \left(\frac{\partial\phi}{\partial z} \right)^2 \right]^- + \left[\left(\frac{\partial\phi}{\partial x} \right)^2 + \left(\frac{\partial\phi}{\partial z} \right)^2 \right]^+, \quad (22)$$

where the superscripts $-$ and $+$ represent the lower and upper surface of the foil. The derivatives of the potential due to the wake elements are obtained by summing up their influences, while the foil-induced velocities are

$$u_0(x, 0^\pm) = \lim_{z \rightarrow 0} \frac{1}{2\pi} \int_0^c \gamma(x_1 t) \frac{z}{(x-x_1)^2 + z^2} dx_1 = \left. \frac{\partial\phi_0}{\partial x} \right|_{z=\pm 0} = \frac{\pm \gamma(x)}{2}, \quad (23)$$

$$w_0(x, 0^\pm) = \lim_{z \rightarrow 0} \frac{1}{2\pi} \int_0^c \gamma(x_1 t) \frac{x-x_1}{(x-x_1)^2 + z^2} dx_1 = \left. \frac{\partial\phi_0}{\partial z} \right|_{z=\pm 0}, \quad (24)$$

here $\partial\phi_0/\partial z|_{z=\pm 0}$ is defined by equation (13).

The time derivative of the potential is

$$\frac{\partial}{\partial t} \phi(x, 0^\pm) = \frac{\partial}{\partial t} \int_{(0, \pm 0)}^{(x, \pm 0)} u dx = \frac{\partial}{\partial t} \int_0^x \left(\frac{\pm \gamma(x)}{2} + u_w^\pm + u_s^\pm \right) dx \quad (25)$$

where u_w and u_s are the trailing edge and the separated wake-induced velocities, respectively. As the various derivatives of the velocity potential are found, the normal force distribution of equation (21) is integrated.

$$F(t) = \int_0^c \frac{dF}{dx} dx = \pi\rho c \left\{ \left[A_0 V_\infty U + \frac{3c}{4} \frac{d}{dt} (A_0 V_\infty) \right] + \left[\frac{1}{2} A_1 V_\infty U + \frac{c}{4} \frac{d}{dt} (A_1 V_\infty) \right] + \frac{c}{8} \frac{d}{dt} (A_2 V_\infty) \right\} + \frac{\rho}{2} \int_0^c \Delta dx. \quad (26)$$

The lift and drag coefficients are

$$C_L = \frac{F \cos \alpha}{\frac{1}{2} \rho V_\infty^2 c}, \quad C_D = \frac{F \sin \alpha}{\frac{1}{2} \rho V_\infty^2 c}. \quad (27), (28)$$

In the calculation of the drag coefficient, the 'thin plate leading-edge suction force' was neglected. This leads to better agreement with high angle-of-attack experimental results, as pointed out by Kiya & Arie (1977).

3. The vortex wake and method of solution

The strength of the two nascent vortices at each time interval was calculated by equations (6) and (7). The upper and lower components of the shear velocity V_u and V_l are calculated by summing up all the velocity components at those points (figure 1):

$$V_u = (V_\infty + V_f + V_w + V_s)_u, \quad (29)$$

$$V_l = (V_\infty + V_f + V_w + V_s)_l, \quad (30)$$

where V_f , V_w , and V_s are the foil, wake, and separated wake-induced velocities, respectively. The latest separated vortice γ_s^i is found according to equation (6)

$$\gamma_s^i = \frac{\Delta\Gamma_s}{\Delta t} \Delta t = C_1 \left(\frac{u_{sh}^2}{2} \Big|_{t-\Delta t} + C_2 \Delta \frac{u_{sh}^2}{2} \Big|_t \right) \Delta t \quad (31)$$

where

$$u_{sh}^2 = V_u^2 - V_l^2. \quad (32)$$

This particular scheme was used because it stabilized the iteration procedure involved with the calculation of the trailing edge wake-shedding process (will be explained later in this text).

The coefficient C_1 is a circulation reduction factor which was used by several authors in order to get better agreements with experiments (Mendenhall & Spangler 1979). In the above work, as well as in the present work, $C_1 = 0.6$ was assumed. However, there are some other methods of achieving wake-circulation reduction, as has been demonstrated by Sarpkaya & Shoaff (1979). They introduced a wake-rediscretization method that reduced the vorticity of the vortices in the proximity of boundaries or other vortex elements. In addition, their method reshaped the roll-up process, thus producing a smoother wake roll-up scheme. The effect of those various methods on the Strouhal number is still to be determined. Since the major scope of the present study is to show a simple simulation of two-dimensional airfoil data over a wide range of angle of attack, the wake circulation reduction was not studied in detail, however, further studies must include such considerations.

The coefficient C_2 of equation (31) was introduced owing to numerical considerations in order to allow a flexible location for the measurement of the shear velocity components V_u and V_l (see figure 1). It was found that a too close positioning of those points to the vortex sheet leads to strong fluctuations in the shear velocity. The relocation of those points at a distance in each side of the separated wake, combined with the amplification factor C_2 , resulted in a stable periodic wake shedding. For the calculated results, shown later on, the time intervals $0.05 \leq \Delta t \cdot V_\infty/c \leq 0.2$ were used with the corresponding values of $8.0 \geq C_2 \geq 3.5$.

The strength of the latest vortex shed at the trailing edge γ_w^i is determined by equation (7):

$$\frac{\Delta\Gamma}{\Delta t} = \frac{\Delta\Gamma_f}{\Delta t} + \frac{\Delta \left(\sum_{n=1}^i \gamma_s^n \right)}{\Delta t} + \frac{\Delta \left(\sum_{n=1}^i \gamma_w^n \right)}{\Delta t} = 0, \quad (33)$$

where γ_s^n and γ_w^n are the separated and trailing-edge vortex elements. The foil circulation Γ_f is calculated by a chordwise integration of the foil circulation,

$$\Gamma_f(t) = \int_0^c \gamma(x) dx = V_\infty(t) \left[A_0(t) \pi + A_1(t) \frac{\pi}{2} \right]. \quad (34)$$

Since equation (33) is fulfilled at any t , the calculation of the nascent vortex is simplified:

$$\gamma_w^i = -(\Delta\Gamma_f + \gamma_s^i). \quad (35)$$

The bound vortex strength Γ_f of equation (34) is dependent on the influence of the wake (including the latest vortices) through boundary condition (13). Therefore, the

strength of the latest vortex shed at the trailing edge was calculated iteratively by the Newton-Raphson method (to fulfil equation (35)):

$$(\gamma_w^i)_{j+1} = (\gamma_w^i)_j - \left[\frac{F(\gamma_w^i)}{\partial F(\gamma_w^i)/\partial(\gamma_w^i)} \right]_j, \quad (36)$$

where j counts the iterations at each time step, and $F(\gamma_w^i)_j$ is defined as

$$F(\gamma_w^i)_j = \frac{d\Gamma}{dt} = \left[\Gamma_f(\gamma_w^i) + \left(\gamma_w^i + \sum_{n=1}^{i-1} \gamma_w^n \right) + \sum_{n=1}^i \gamma_s^n \right]_j. \quad (37)$$

Convergence to accuracy of 0.1 % is obtained within a 3–5 iteration.

For the case where the foil vorticity is represented by discrete vortices, this iterative scheme is not required. This method was not adopted in the present work since that approach might result in higher computational times for similar accuracies.

The time-dependent solution of the flow field at any time interval is attained as follows. First, the foil downwash distribution (13) is calculated while assuming known strength of nascent vortices. Then the foil circulation is solved by integrating (19) and (20). Finally, the latest separated vortex strength was calculated using (31), while the strength of the nascent trailing-edge vortex was iterated as in (36).

As the solution for the vortices' strength is found, the pressure distribution and forces are evaluated (26). The range of time interval Δt used was

$$0.05 < (\Delta t \times V_\infty)/c < 0.2,$$

and the main variation observed in that interval was a slight increase in Strouhal number, with the reduction of time step. As the momentary flow field is solved, the wake shedding and convection is performed. At each time interval, the vortices are placed midway along the path covered by the separation points during that period. This vortex positioning seems to minimize numerical error due to vortex sheet discretization, at the vicinity of curved streamlines (Clements 1973). The momentary vortex roll-up at any time step was obtained by the corresponding motion of each vortex element along the foil wakes-induced streamlines.

In the present work, special procedures designed to save computer time, such as vortex combination (Kiya & Arie 1977; Sarpkaya 1975), were not used since computational times were minimal (less than 20 s CDC-7600 for the data appearing in figures 2–5).

The oscillation of the separation point that plays an essential role in the actual oscillatory wake shedding by the viscous boundary layer (Sarpkaya 1975) was achieved by applying a 'Kutta-type' condition at the separation point. That condition introduced a slight vertical displacement of the nascent vortex to fulfil the zero-slip condition at the separation point.

An extension of the present work to include the foil thickness effect can provide a better computational scheme for the separation point, whereas the experimental information is still very limited.

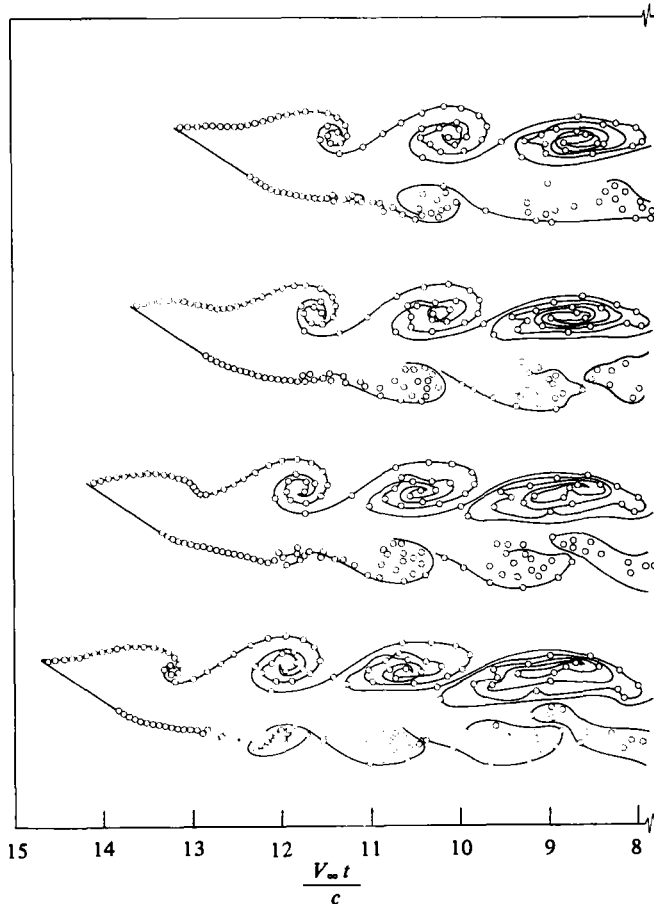


FIGURE 2. Vortex pattern behind a separated symmetrical airfoil.
 $\alpha = 30^\circ$, $V_\infty \Delta t/c = 0.1$, $X_{sep}/c = 0.05$.

4. Results for periodic wake shedding

The periodic wake shedding behind an inclined airfoil with a separation point at $X_{sep}/c = 0.5$ is shown in figure 2. It is assumed that the foil leading edge is rounded and the separation is developed by a gradual forward motion of the separation point along the chord (starting at the trailing edge) when increasing the angle of attack. The four diagrams of figure 4 show that the upper vortex sheet conglomeration and chronological order is less disturbed than the roll-up of the lower sheet. That is due to the rather uniform flow above the foil, while the lower roll-up process is distorted by the already rolled-up upper sheet. The drifting motion of the wake behind the foil has a stretching effect on the discrete vortex concentration, resulting in further distortions in the roll-up process. Apart from those distortions and numerical errors, there is an additional instability (Batchelor 1970). This instability is developing as the tangential velocities at the core of a highly rolled-up vortex concentration are increasing and the centrifugal forces are resulting in a vortex breakdown. The numerical accuracy of the above wake-calculation method was demonstrated by Katz &

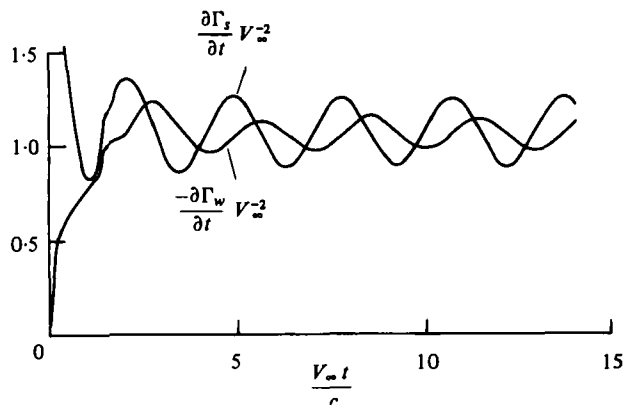


FIGURE 3. Rate of vorticity shedding (assuming constant $X_{sep} = 0.05c$ from the start of the motion). $\alpha = 30^\circ$.

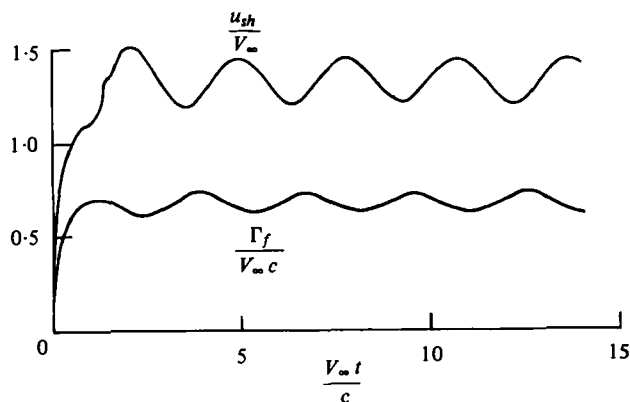


FIGURE 4. Periodic variation of shear velocity and foil circulation. $X_{sep}/c = 0.05$, $\alpha = 30^\circ$.

Weih's (1978*b*) who showed good agreement between calculated wake shapes behind non-separated oscillating airfoils and flow visualizations.

The above numerical vortex wake roll-up calculations show similarity to existing flow-visualization experiments, such as Fage & Johansen (1927) or McAlister & Carr (1978). Corresponding flow visualization for the calculated wake shapes of figure 2 has not been conducted so far at Ames' Water Tunnel owing to strong three-dimensional effects. Similar difficulties at high-angle-of-attack flow visualization were reported by Moss & Murdin (1968).

The time-dependent vorticities and force coefficients are plotted in figures 3–5. The foil was suddenly set into motion and the oscillatory data were computed. The separation point was set from start to be at $X_{sep}/c = 0.05$, whereas the motion of that point should actually have been started at the trailing-edge vicinity and gradually moved forward. Since the purpose of those calculations was to demonstrate the process of achieving periodic oscillation, the exact physics of the sudden acceleration were not investigated.

Figure 3 shows the vorticity shed from the separation point and from the trailing edge. The non-symmetric wake shedding shown is a result of Kelvin's theorem applied

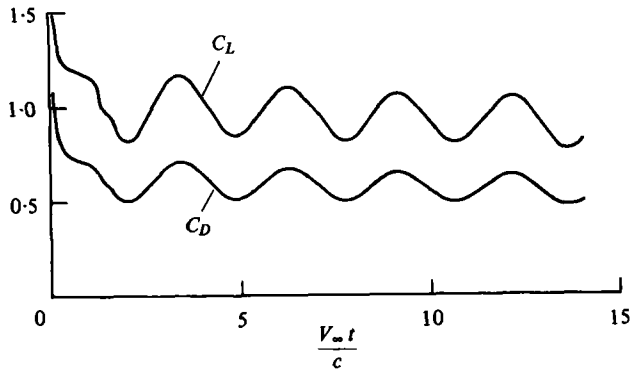


FIGURE 5. Periodic variations of lift and drag coefficients. $X_{sep}/c = 0.05$, $\alpha = 30^\circ$.

in the present model. That is, the foil circulation (figure 4) varies in such a way that there is zero net circulation generation at all t . The shear velocity oscillations u_{sh}/V_∞ of the separated wake in figure 4 also have a sinusoidal shape, unlike the calculated results of Kiyama & Arie (1977).

Figure 5 shows the periodic variation of the lift coefficient C_L and drag coefficient C_D . The phase is shifted from that of the foil circulation on figure 4. This is a result of the $\partial\phi/\partial t$ term in equation (21). The Strouhal number ($St = 0.18$) for this calculation is in close agreement with several experimental results. Here the Strouhal number has been defined as

$$St = \frac{fc \sin \alpha}{V_\infty} \quad (38)$$

where f is the wake-oscillation frequency. Fage & Johansen (1927) found values about $St = 0.148$ for flat plates, while Roshko (1954) showed that a universal wake-based Strouhal number (including flow over separated flat plates) has the value of $St = 0.15$ – 0.18 . Both of these works investigated separation patterns similar to a sharp leading-edge flat-plate separation. In the present work, however, it is assumed that the flow moves around the leading edge and separates only at a further point, resulting in a smaller wake cross-section. This results in a universal St number that is close to Roshko's (1954) results.

5. High-angle-of-attack airfoil data calculation

In order to demonstrate the ability of the method, two different types of airfoil data were simulated. The only input for the calculation was the separation point location. This location is generally a function of Reynolds number and geometry (foil curvature and angle of attack) and might be obtained by either experimental flow visualization or calculated by some separation criteria.

Figures 6 and 7 show several aerodynamic parameters of an airfoil (NACA 0012) as a function of angle of attack, for $Re = 1.8 \times 10^6$. The simulation was done by assuming a fully attached flow ($X_{sep} = 1$, on figure 7)† up to $\alpha = 14^\circ$ and an almost

† For the input of $X_{sep} = 1$, the computer code assumes $d\Gamma_s/dt = 0$ and performs a linear thin-wing calculation (as in Katz & Weihs 1978a).

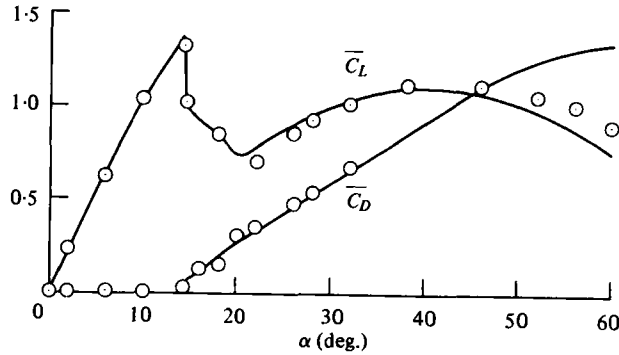


FIGURE 6. Calculated data for wide range of angle of attack for airfoil section NACA 0012. \circ , Critzos *et al.* (1955), two-dimensional results for $Re = 1.8 \times 10^6$; —, present calculation.

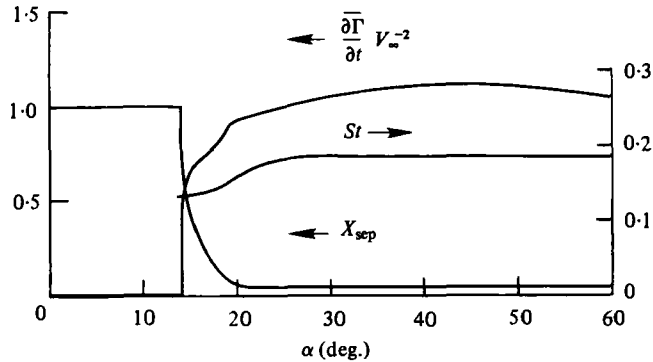


FIGURE 7. The assumed motion of separation point for an airfoil section NACA 0012 and resulting shear-layer strength and Strouhal number. —, theory.

complete separation ($X_{sep} = 0.05$) for $\alpha > 20^\circ$. At the intermediate region

$$14^\circ < \alpha < 20^\circ,$$

X_{sep} was chosen to fit the foil data. The experimental points stand for the data measured by Critzos, Heyson & Boswinckle (1955) and seem to follow reasonably the theoretical time average lift \bar{C}_L and drag \bar{C}_D coefficient values in figure 6. The average rate of vorticity shed at either separation point $\partial \bar{\Gamma} / \partial t$, as a function of angle of attack, is shown in figure 7. The Strouhal-number prediction seemed to be constant for a wide range of α , and slightly lower in the angle-of-attack range for partial separation. (The author found no experimental information about this region.)

Figures 8 and 9 show calculation and experimental results for the cambered NACA 63₂-415 section that is being used on several general aviation aircraft. Here the separation starts to develop at low angles ($\alpha = 8^\circ$) and then gradually moves forward, as angle of attack increases, resulting in higher lift losses (figure 9). That process continues until a sharp forward motion of the separation point occurs at $\alpha = 18^\circ - 19^\circ$. Then this motion advances until $\alpha = 22^\circ$ where full separation is obtained.

The time-average lift and drag coefficients are plotted in figure 8. The triangle represents the airfoil data obtained by Abbott, Doenhoff & Stivers (1945). In general, there are very little experimental data available on post-stall characteristics of airfoils.

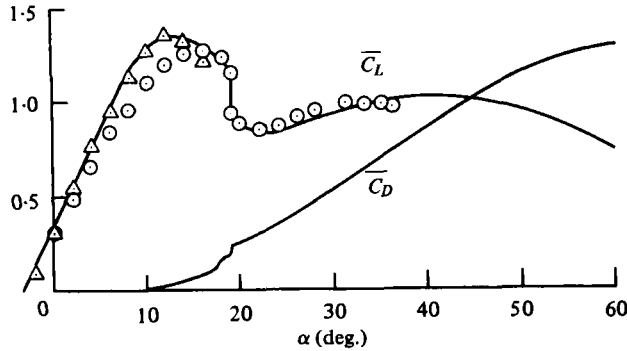


FIGURE 8. Calculated data for wide range angle of attack for airfoil NACA 63₂-415. Δ , Abbott *et al.* (1945), two-dimensional results for $Re = 6 \times 10^6$; \circ , Feistel *et al.* (1978), aspect ratio = 7.5, $Re = 1.5 \times 10^6$; —, present calculation.

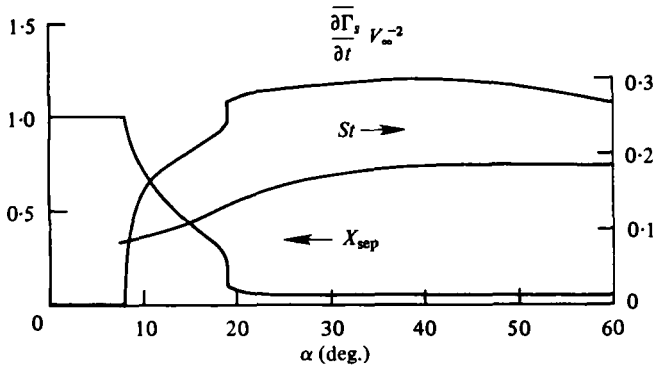


FIGURE 9. The assumed motion of separation point for an airfoil section NACA 63₂-415 and resulting shear-layer strength and Strouhal number. —, theory.

For that reason, the circles in figure 8 represent the only other data known to the author about that airfoil. This experiment was conducted at the Ames 7- by 10-foot wind tunnel in connexion with the aircraft post-stall studies of Feistel *et al.* (1978). The wing section was tested at Reynolds number 1.5×10^6 and had an aspect ratio of 7.5. Three-dimensional wing correction for those data was not made, since this correction is expected to be smaller at the separated flow region than it is in the linear region.

The average strength of the vorticity shed at the separation points $\partial\bar{\Gamma}/\partial t$ and the Strouhal number are plotted in figure 9. In this case too, for the angle-of-attack range of the partial separation, a reduction in Strouhal number is indicated as in figure 7.

6. Conclusion

The two-dimensional discrete-vortex method shown here has been successfully used to simulate airfoil section lift and drag data over a wide range of angle of attack. Furthermore, the periodically varying forces and vortex-wakes' roll-up has been calculated. This method of representing airfoil data can be used as an integral part of a three-dimension vortex lattice panelling method, where the influence of separated flow on the attached region is to be calculated. The inclusion of thickness effect with

established separation criteria should lead to a further improvement in the above results by allowing the calculation of the separation point for given Reynolds number and foil geometry.

REFERENCES

- ABBOTT, I. H., DOENHOFF, A. E. & STIVERS, L. S. 1945 Summary of airfoil data. *N.A.C.A. Rep.* no. 824.
- BACHELOR, G. K. 1970 *An Introduction to Fluid Dynamics*. Cambridge University Press.
- CLEMENTS, R. R. 1973 An inviscid model of two-dimensional vortex shedding. *J. Fluid Mech.* **57**, 321-336.
- CLEMENTS, R. R. & MAULL, D. J. 1975 The representation of sheets of vorticity by discrete vortices. *Prog. Aerospace Sci.* **16**, 129-146.
- CRITZOS, C. C., HEYSON, H. H. & BOSWINKLE, R. W. 1955 Aerodynamic characteristics of NACA 0012 airfoil section at angles of attack from 0° to 180° . *N.A.C.A. Tech. Note* 3361.
- FAGE, A. & JOHANSEN, F. C. 1927 On the flow of air behind an inclined flat plate of infinite span. *Proc. Roy. Soc. A* **116**, 170-197.
- FEISTEL, T. W., ANDERSON, S. B. & KROEGER, R. A. 1978 A method for localizing wing flow separation at stall to alleviate spin entry tendencies. *A.I.A.A. Paper* 78-1476.
- KATZ, J. & WEIHS, D. 1978a Hydrodynamic propulsion by large amplitude oscillations of an airfoil with chordwise flexibility. *J. Fluid Mech.* **88**, 485-497.
- KATZ, J. & WEIHS, D. 1978b Behavior of vortex wakes from oscillating airfoils. *J. Aircraft* **15**, 871-863.
- KIYA, M. & ARIE, M. 1977 A contribution to an inviscid vortex-shedding model for an inclined flat plate in uniform flow. *J. Fluid Mech.* **82**, 223-240.
- MCALISTER, K. W. & CARR, L. W. 1978 Water tunnel experiments on an oscillating airfoil at $Re = 21000$. *N.A.S.A. TM-78446*.
- MCCULLOUGH, G. B. & GAULT, D. E. 1951 Examples of three representative types of airfoil section stall at low speed. *N.A.C.A. TN-2502*.
- MARSHALL, F. J. & DEFFENBAUGH, F. D. 1974 Separated flow over bodies of revolution using an unsteady discrete-vorticity cross wake. *N.A.S.A. CR-2414*.
- MENDENHALL, M. R., SPANGLER, S. B. & PERKINS, S. C. 1979 Vortex shedding from circular and noncircular bodies at high angles of attack. *A.I.A.A. Paper* 79-0026.
- METHTA, B. U. 1977 Dynamic stall of an oscillating airfoil. *AGARD Fluid Dynamics Panel Symp. on Unsteady Aerodynamics, Ottawa, Canada*, Paper 22.
- MOSS, G. F. & MURDIN, P. M. 1968 Two-dimensional low speed tunnel tests on the NACA 0012 section including measurements made during pitching oscillations at the stall. *R.A.E. Tech. Rep.* no. 68104.
- PINKERTON, R. M. 1937 The variation with Reynolds number of pressure distribution over an airfoil section. *N.A.C.A. Rep.* no. 613.
- ROSHKO, A. 1954 On drag and shedding frequency of two-dimensional bluff bodies. *N.A.C.A. TN-3169*.
- SARPKAYA, T. 1975 An inviscid model of two-dimensional vortex shedding for transient and asymptotically steady separated flow over an inclined plate. *J. Fluid Mech.* **68**, 109-128.
- SARPKAYA, T. 1979 Vortex-induced oscillations. *J. Appl. Mech.* **46**, 241-258.
- SARPKAYA, T. & SHOAFF, R. L. 1979 An inviscid model of two-dimensional vortex shedding for transient and asymptotically steady separated flow over a cylinder. *A.I.A.A. Paper* 79-0281.
- SEARS, W. R. 1976 Unsteady motion of airfoils with boundary-layer separation. *A.I.A.A. J.* **14**, 216-220.
- STRATFORD, B. S. 1959 The prediction of separation of the turbulent boundary layer. *J. Fluid Mech.* **5**, 1-16.